CHAPTER-5

Highly efficient FeNP-embedded hybrid bifunctional reduced graphene oxide for Knoevenagel condensation with active methylene compounds

[5.1] Introduction

The formation of carbon-carbon bond via Knoevenagel condensation reaction of aldehyde/ketone with compounds containing activated methylene groups is being paid a great contemplation by the researchers because of its deployment in synthesis of fine chemicals, [1] therapeutic drugs, [2] natural products [3] and functional polymers. [4] Typically, this base catalyzed organic reaction is of great magnitude in the chemical process industry, which plays a vital role in achieving higher aldehyde conversion. [5] In the last few decades, the Knoevenagel condensation reaction has conventionally been performed by soluble base catalysts such as aliphatic amines, urea, thiourea, and piperidine or their corresponding ammonium salts and/or amino acids. Despite of having distinct advantages the aforesaid system suffered from several snags such as easier separation, longer reaction time, un-satisfactory yields, reusability, high costs, harsh reaction conditions as well as the use of stoichiometric amounts of catalyst. [6]

Now-a-days, frontier scientific and technological research field has been spotlighted on solid supported base modified catalysts, which can be adequately applied for condensation reactions giving better yield and stability besides the first-rate conversion with the desired selectivity. Discrete types of heterogeneous base modified catalytic systems have been flourished such as amino-functionalized mesoporous silica, [7] diamine-functionalized mesopolymers, [8] Amine functionalized K10 montmorillonite, [9] super paramagnetic mesoporous Mg–Fe bi-metallic oxides, [10] mesoporous titanosilicate, [11] basic MCM-41 silica, [12] acid-base bifunctional mesoporous MCM-41 silica, [13] nanocrystalline ceria-zirconia, [14] zeolites exchanged with alkylammonium cations, [15] Cu(II)-based metal-organic framework, [16] chitosan hydrogel, [17] acrylic resin immobilized lipase, [18] organic-inorganic hybrid silica materials containing imidazolium and dihydro imidazolium salts, [19] IRMOF-3, [20] and ZIF-8. [21] In contrast, these base solid catalysts have endured from a number of downsides such as high temperature, longer reaction time, poor selectivity and tedious work-up procedures.

At the present time, the potent and sophisticated heterogeneous catalysts with a tunable multifunction are in strong demand in the area of green and sustainable science and technology. The combination of both acidic and basic sites employed in designing and advancing of heterogeneous catalysts with bifunctional assets is of ongoing interest in organic synthetic chemistry. Bifunctional catalysts can competently upshot a wide range of molecular transformation including C–H, C–C, C–O, or C–N bond formation and have attention up to great extent in proficiently catalyzing a wide range of reactions, such as one-pot cascade reactions, [22–24] transfer hydrogenation reactions, [25] nucleophilic addition reactions, [26] C-C bond formation reaction [27–29] and so on. This can be made achievable by dual activation and effectual accrual of reacting substrates on the adjoining active centers in the same species. The active sites in the bifunctional catalyst on the solid surface must be array in such approach that they do not make any amendment with their functions but act autonomously and sometimes co-operatively leading to a unique activity.

Up till now, several attempts have been made on heterogeneous catalytic systems to develop multifunctional acid-base catalysts for diverse reactions, for instance, recently Z. Jiang and co-workers [30] have reported a trouble-free route for the fabrication of acid-base HPA catalyst used in transesterification of TGs and esterification of FFAs for biodiesel production. H. Liu et al. [31] have explored the acid-base bifunctional catalytic activity of phosphor-doped h-BN nanosheets (BNP) by catalyzing deacetalization–Knoevenagel cascade reactions successively in a single pot. The bifunctional amphiphilic organic nanotube (acid–base-nanotube) containing 1-(2-(prop-2-yn-1-yloxy)ethyl)-1*H*-imidazole (PEI) groups as basic sites and benzenesulfonic acid (BSA) groups as acidic sites on the corona of nanotube has been developed by K. Huang and co-workers. [32] The catalytic activity of multisite acid-base-nanotube catalyst has shown a higher conversion of benzaldehyde dimethyl acetal in deacetalization-Knoevenagel cascade reactions sequentially in a single pot. M. Abdouss et al. [33] have fabricated heterogeneous catalyst such as GO-SO₃H and has exclusively

promoted for one-pot cyanosilylation of aldehydes with TMSCN with superior activity, giving valuable multifunctionalized cyanohydrin trimethylsilyl ethers.

In these days and age, functionalized graphene nanosheets have been explored as a supported material in catalyzing diverse organic transformation reactions due to its large specific surface area (~2630 m^2/gm), rich oxidative debris (like –OH, -COOH, -C-O-C, -C=O groups) as well as fascinating physical properties (electronic, mechanical and thermal). [34–37] Besides this, it also possess elevated tensile and mechanical strength which makes the catalyst more stronger and able to resist the acidic and basic media produce either during the reaction or necessitate for to make the reaction happen [34] and In addition to this, it also facilitates high mass transfer reaction For this reason we have chosen GO. The expediency of the substrates over active surface is amplified by the presence of surface oxidative debris as in case of GO/rGO. This contributes to augment dispersion of metal or metal-oxide nanoparticles onto GO/rGO surface, endow with Lewis acidic sites. [38–40] Besides these rich oxygenated debris and defects on its surface can play a decisive role as nucleation sites to tether with versatile organic base derivatives via covalent attachment offering basic sites. In recent years, some efforts have been deliberated in the direction of using organoamine derivatives tethered onto the basal plane of GO as base catalysts for Knoevenagel condensation reaction. [41] For instance, make use of 3-aminopropyl-triethoxysilane (APTS) as the organic base, N. Zhang and co-workers [42] conveniently developed APTS functionalized GO catalyst (GO-APTS) and used for Knoevenagel condensation reaction. This catalyst has shown exceptional performance with >90% yield and also tested to extensive range of substrates.

As a consequence of tackling this exigent issue, the development of newfangled bifunctional catalyst became enormous significant for us. In continuation to our ongoing research, [43] in this work, we report highly efficient bifunctional FeNPs anchored on amino modified reduced graphene oxide nanocatalysts (FeNPs/Am@rGO) [where, Am = *P*-phenylenediamine (PPD) and/or aniline (AN)]. The accountability of rGO in the synthesized nanocatalysts

is predominantly as a supported material due to enhancing the mechanical strength of the catalysts and also provides its surface to the substrate molecule to be easily adsorbed, which aids in easy recoverability and recyclability of the catalysts. [44, 45] These bifunctional nanocatalysts have been tested over Knoevenagel condensation reaction with different aromatic aldehydes and active methylene compounds (ethyl acetoacetate, ethyl cyanoacetate and malononitrile). The impact of discrete parameters influencing catalytic activity such as catalyst amount, mole ratio, solvent, temperature and time have also been monitored.

[5.2] Expermentals Section

(a) Materials

Malononitrile (MLN), Ethyl cyanoacetate and Ethyl acetoacetate was procured from Spectrochem Pvt. Ltd. Other chemicals such as $FeCl_3$ anhydrous, Aniline, $NaBH_4$, were procured from S D Fine Chem Ltd. *p*-Phenylenediamine was purchased from High Purity Laboratory Chemicals Pvt. Ltd. All the materials are of analytical grade and used as received without further purification.

(b) Synthesis of graphene oxide (GO)

Graphene oxide was synthesized from graphite flakes using a modified Hummer's method. [46]

(c) Synthesis of Amino modified graphene oxide (Am@GO) nanocatalyst

P-phenylenediamine (PPD) and/or aniline (AN) was used to functionalize GO and as a result of this functionalization, $-NH_2$ group was tethered onto the surface of GO viz. PPD@GO and/or AN@GO. 500 mg GO was dispersed in 100 mL distilled water using ultrasonic treatment for 10 min. Then, 1 g of *p*-phenylenediamine and/or aniline in 10 ml of acetone was added drop-wise in the suspension of GO and the suspension mixture was allowed to stir for 12 h at room temperature. The resulting solid mixture was separated by centrifugation and the product was washed with acetone and water which was later dried in a vacuum oven for 48 h.

(d) Synthesis of Fe/Am@rGO nanocatalysts

As-prepared 20 mg Am@GO viz. PPD@GO and/or AN@GO was dispersed in 10 mL of distilled water using ultrasonic treatment for 30 min at room temperature. It was followed by drop wise addition of 2 mmol of aqueous solution of $FeCl_3$ into the suspension of Am@GO which was ultrasonicated for 20 min to produce homogeneously dispersed suspension. After being sonicated, a freshly prepared solution of $NaBH_4$ (5 ml) was added drop by drop into the suspension and solution mixture was stirred constantly for 30 min at room temperature. Finally, black precipitates of nanocomposite materials were obtained that signifies the successful reduction of Fe to FeNPs and GO to rGO. The solid product was separated by centrifugation and washed with distilled water, later dried in an air oven at 65 ^{o}C.

(e) Catalytic test

In a typical Knoevenagel condensation reaction experiment, a mixture of 5 mmol benzaldehyde, 5 mmol active methylene compound viz. malononitrile, 5 mL toluene and 20 mg (0.11 mol% of Fe) catalyst were added into a 50 mL round bottom flask at 40 °C and the reaction mixture was kept under vigorous stirring. After completion of the reaction, solvent was recollected by rotary evaporation under the vacuum. The organic aliquot was analyzed by a Chemito 8610 gas chromatography (GC) equipped with DB-5 capillary column (30 m, 0.32 mm id, 0.25 μm film thickness). The recovered catalyst was washed with ethanol followed by distilled water, later dried in hot air oven at 80 ^{o}C for 6 h before reuse.

[5.3]   Results and discussion

The purpose of this work was to synthesize heterogeneous bifunctional nanocatalysts through functionalizing graphene nanosheet with p-phenelynediamine and/or aniline followed by FeNPs embedded onto the surface of rGO by reduction-deposition method. These heterogeneous bifunctional nanocatalysts were employed for Knoevenagel condensation reaction with

different aromatic aldehydes and active methylene compounds. The as-prepared nanocatalysts schematic representation, characterization and their catalytic aptitude are discussed as shown below:
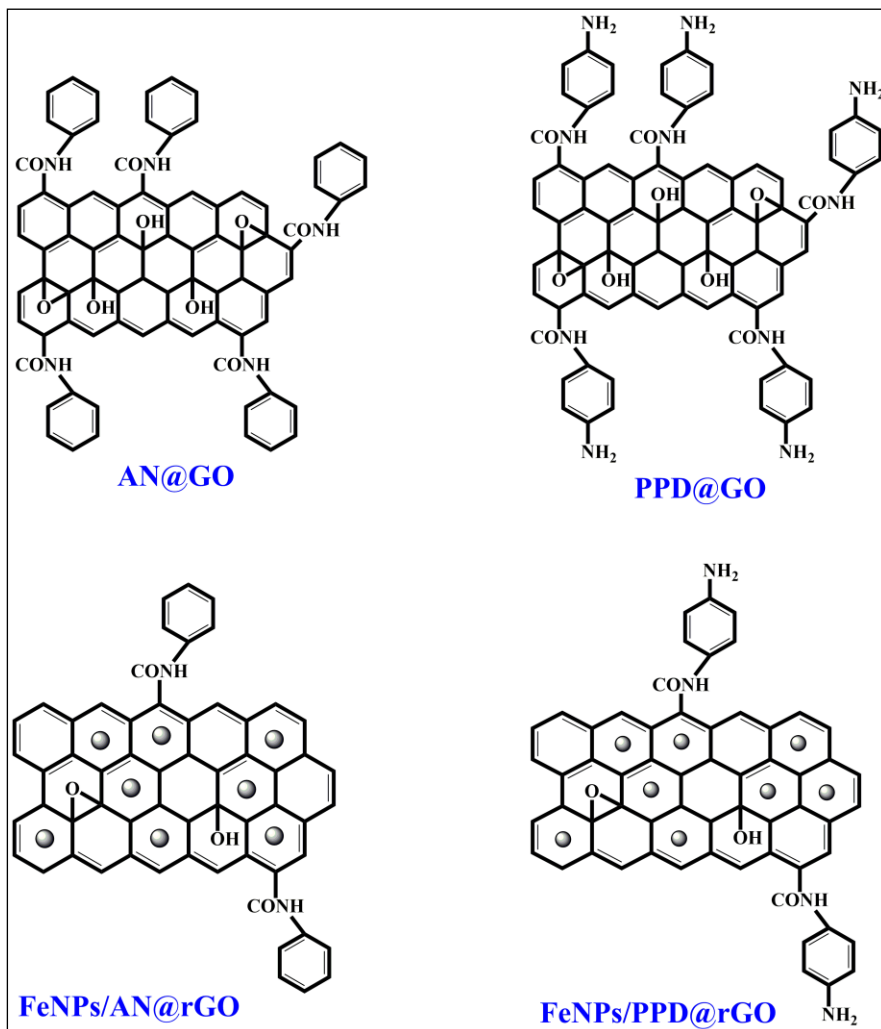
Scheme 1 Schematic representative of used nanocatalysts GO, AN@GO, PPD@GO, FeNPs/AN@rGO, and FeNPs/PPD@rGO

❖ **Characterization of nanocatalysts**

(a) **Raman spectra:**

As a nondestructive and noninvasive chemical analysis technique, the Raman spectroscopy is evolving into one of the most useful technique for the characterization of lattice structure and morphological changes during the

synthesis of nanocatalysts. [47–49] Raman spectra of heterogeneous bifunctional nanocatalysts such as FeNPs/AN@rGO and FeNPs/PPD@rGO are shown in Fig. 1. The positions, line shapes, and two prominent intensities of peaks (D band and G band) strongly dominate on the microstructure of nanocrystalline materials. Where D-band attributed to the symmetry forbidden band of the longitudinal plane phonon vibration or k-point phonons of A_{1g} symmetry and G-bands corresponds to the long-wavelength longitudinal phonon mode of graphene (E_{2g} phonon) arises due to the sp^2 carbon network of the graphene plane, respectively. [50] It was observed that both D and G bands of as-synthesized compounds of GO (depicted chapter 2, fig. 10), shifts to a slightly lower frequency, was believed to be due to high exfoliation of sheets. [51] Here, the intensity ratio of D to G band (I_D/I_G) for AN@GO and PPD@GO were 1.07 and 1.10, respectively. Furthermore, I_D/I_G ratio of FeNPs/AN@rGO and FeNPs/PPD@rGO was superior to that of GO (depicted in chapter 2, figure X), AN@GO and PPD@GO. This augmentation might be due to the insertion of organoamino derivatives and metal ion onto the basal and/or edges sites of rGO nanosheet. Furthermore, the as-synthesized FeNPs/PPD@rGO and/or FeNPs/AN@rGO compounds may create a large number of graphitic domains; albeit, these graphitic domains are smaller in size compared with GO.[52,53] The blue shifting of G band indicates the softening of phonons which may occur due to electron enrichment in the GO sheets and therefore can be easily migrated the charge to organic moiety and metal ion. In addition to this, we have also evaluated crystalline size and inter defect distance of AN@GO, PPD@GO, FeNPs/AN@rGO, and FeNPs/PPD@rGO nanocomposites by the Tuinstra-Koenig relations, using this equation are calculated to be 17.9, 17.4, 17.3 and 16.8 nm, respectively.[54,55]
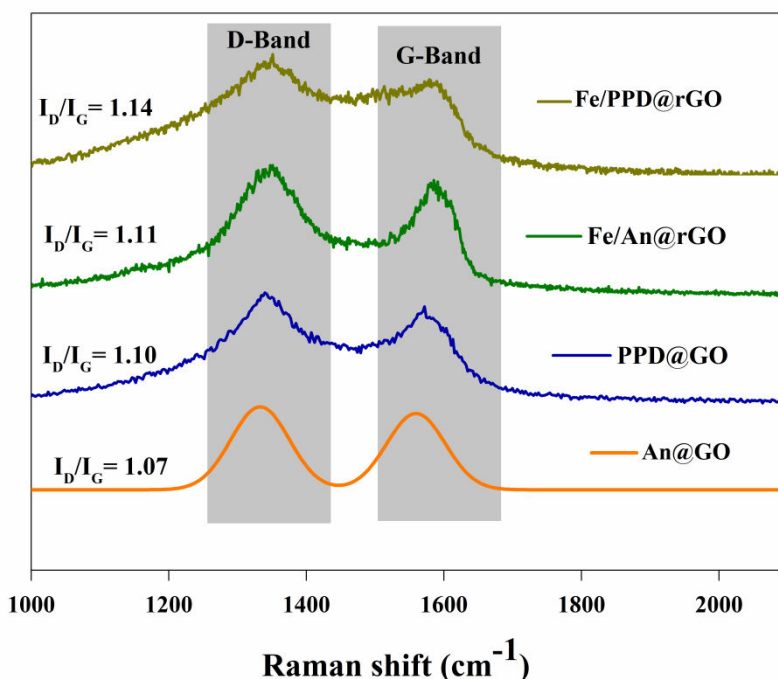
Figure 1 Raman spectra of AN@GO, PPD@GO, FeNPs/AN@rGO and FeNPs/PPD@rGO

(b) X-ray diffraction study:

The structural integrity studies were employed to investigate crystallinity of the as-prepared nanocatalysts. Fig. 2 exhibits powder XRD patterns of AN@GO, PPD@GO, FeNPs/AN@rGO, and FeNPs/PPD@rGO. For GO, all details such as diffraction peak and interlayer distance are given chapter 2, fig. 8. [56–58] Furthermore, on reaction with AN and PPD, these moieties were inserted between the GO nanosheets via forming -CONH- groups. Here, PPD contains two NH_2 groups at the C-1 and C-4; while, aniline possesses only one NH_2 group at C-1 position. Therefore, it is obvious that in PPD@GO, the inter-planar distance is higher than AN@GO and it was substantiated by the inter-planar distance calculation using Debye‑Scherrer equation viz. 3.8 and 3.5, respectively. Moreover, during *in situ* grafting of Fe nanoparticles and reduction of GO nanosheets, the inter-planar distance further expected to decrease (slightly in both the cases). But in compared to FeNPs/AN@rGO, it remains higher in FeNPs/PPD@rGO. As a result, in FeNPs/AN@rGO catalyst, rGO nanosheets are

tend to aggregate and formation of stacked layer arrangement. Because of this restacking, it showed a characteristic peak at ~23; while it was disappeared in FeNPs/PPD@rGO indicating the more exfoliated layered structure. [59–62] The Bragg reflection at 29.1, 34.8, 42.6, 53.8, 57.3, 62.7 and 73.9 (2 theta) in FeNPs/AN@rGO and FeNPs/PPD@rGO corresponds to the (220), (311), (400), (422), (511), (440) and (533) plane of crystallinity of Fe nanoparticles (JCPDS standard 19-0629 of Fe), respectively. Hence, by XRD pattern, the successful attachment of Fe nanoparticles was substantiated in the FeNPs/AN@rGO and FeNPs/PPD@rGO nanocatalysts, [63] which are in a good agreement with surface area electron diffraction (SAED pattern) in HR-TEM analysis [Fig. 3 (E)].
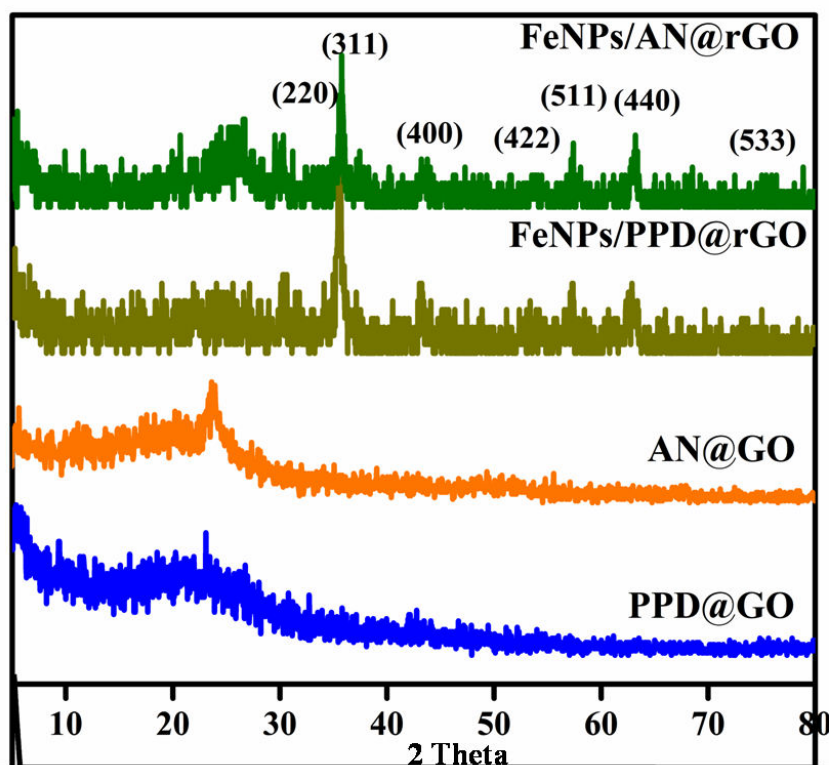

Figure 2 XRD pattern of PPD@GO, AN@GO, FeNPs/PPD@rGO and FeNPs/AN@rGO.

(C) High-resolution transmission electron microscopy (HRTEM)

The size, microstructure and spherical morphology of FeNPs/PPD@rGO nanocatalysts were examined by high-resolution transmission electron microscopy (HRTEM). From Fig. 3 (A and B), it can be observed that the fine

narrow sized Fe nanoparticles (FeNPs) were homogenously dispersed on the PPD@rGO nanosheet. From fig. 3 (C), the size distribution of the FeNPs on the PPD@rGO nanosheet was investigated by Image J software where the average size of the nanoparticles was found to be 4.5 ± 1.6 nm. As can be seen in Fig. 3 (D), FeNPs/PPD@rGO nanocatalyst provides an evidence of the crystal lattice fringes of FeNPs with a d-spacing of 0.23 nm, which can be expressed with the plane of cubic FeNPs. The diffraction spot observed in the SAED image of FeNPs/PPD@rGO [Fig. 3 (E)] confirmed polycrystalline nature of FeNPs on the surface of rGO nanosheet. Moreover, the intense spherical spots of FeNPs observed in SAED pattern are analogous to the XRD results as discussed above.
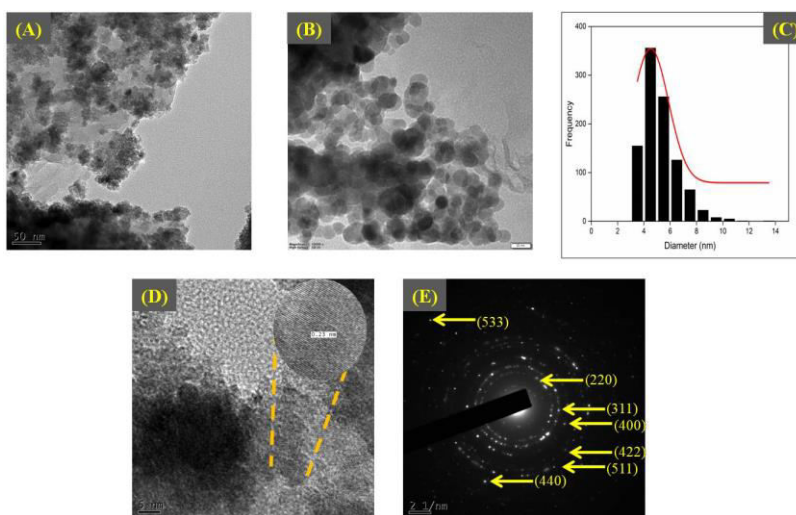

Figure 3 (A) Low magnification of TEM images of FeNPs/PPD@rGO nanocatalyst, (B) HR-TEM images of FeNPs/PPD@rGO nanocatalyst (C) Histogram graph of FeNPs/PPD@rGO (D) HRTEM image of FeNPs/PPD@rGO with fringe spacing, (E) SAED image of FeNPs/PPD@rGO.

(d) Scanning electron microscopy (SEM)

From the SEM image of PPD@GO, GO can be functionalization with PPD [Fig. 4 (a)], roughness of the surface increases suggesting that it alters the surface morphology of GO to more amorphous nature. On the other hand [Fig. 4(b)], embedment of Fe nanoparticles, no further alteration on the surface was seen and the successful attachment of FeNPs on the surface. [64]
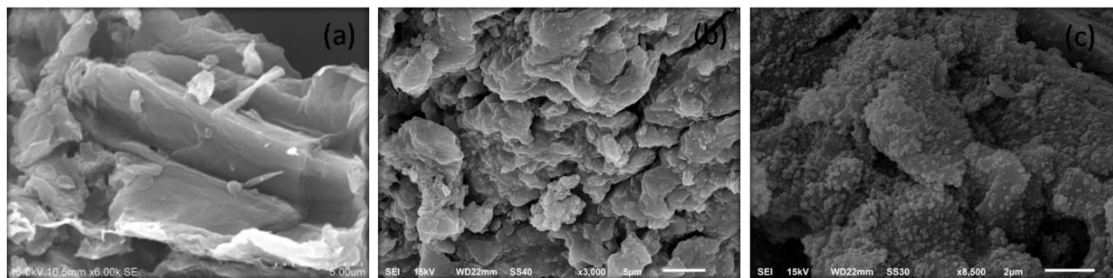
Figure 4 SEM images of (a) PPD@GO, (b) FeNPs/PPD@rGO (adapted from Ref. 82 with permission of Royal Society of Chemistry)

(e) Fourier Transfer Infrared spectroscopy (FTIR)

FTIR spectra of AN@GO, PPD@GO, FeNPs/AN@rGO and FeNPs/PPD@rGO are shown in Fig. 5.The FT-IR spectrum of GO shown in Chpater 2, fig. 6, which compared with AN@GO, PPD@GO, FeNPs/AN@rGO and FeNPs/PPD@rGO. [65, 66] In the FTIR spectra of AN@GO [Fig. 5(B)] and PPD@GO [Fig. 5(C)], three bands monitored at around 3246-3181 cm^{-1}, 2863-2893 cm^{-1} and 1598 cm^{-1} were attributed to υ(N-H), υ(C-H) aromatic and υ(C=C) stretching vibrations, respectively. [67] The presence of stretching vibrations at 1307 and 1308 cm^{-1}, authenticated C–N group in AN@GO and PPD@GO, respectively. When FeNPs adhered onto Am@rGO nanosheet, the C-N band was shifted to lower frequency region at 1294 and 1298 cm^{-1} in FeNPs/AN@rGO and FeNPs/PPD@rGO, respectively. Nonetheless, after the forming of AN@GO, PPD@GO, FeNPs/AN@rGO and FeNPs/PPD@rGO, the carbonyl band was disappeared which clearly indicates the successful functionalization of organoamino derivatives on GO nanosheet.

In the FTIR spectra of FeNPs/AN@rGO and FeNPs/PPD@rGO, the absorption bands observed at 1517 cm^{-1} and 1507 cm^{-1} represent flake like sheet, still remaining after chemical reduction process. [68] Two new bands examined at 581 cm^{-1} and 571 cm^{-1} due to the stretching vibration of Fe-O bond.
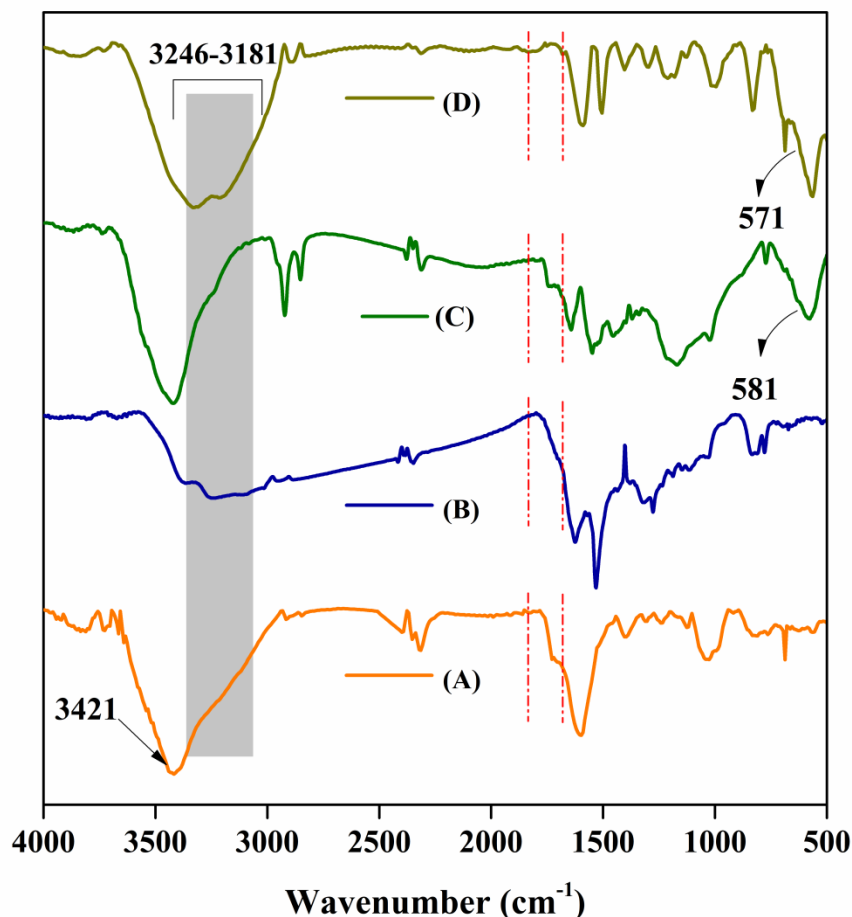
Figure 5 FTIR spectra of (A) AN@GO (B) PPD@GO (C) FeNPs/AN@rGO (D) FeNPs/PPD@rGO

(f) Thermogravimetric analysis (TGA)

The chemical and compositional modifications along with thermal stability of as-prepared materials are reflected in thermogravimetric analysis of AN@GO, PPD@GO, FeNPs/AN@rGO and FeNPs/PPD@rGO (Fig. 6). The thermal analysis of GO depict in chapter 2, fig. 7, which matched with AN@GO, PPD@GO, FeNPs/AN@rGO and FeNPs/PPD@rGO.

While performing comparison among TG diagrams of AN@GO, PPD@GO, FeNPs/AN@rGO and FeNPs/PPD@rGO: AN@GO and PPD@GO showed initial mass loss of about 9.7% and 6.7%, respectively, within the temperature range of 40-100 ^{o}C that corresponds to the liberation of physisorbed

water molecules. The second weight loss of 22.3% and 11.4% occurred in the temperature range of 110-280 ^{o}C, corresponding to the evolution of un-functionalized (not reacting with AN and/or PPD) oxygen-containing functional groups. The concluding stage, weight loss of 63% and 79.6% in the temperature range of 280-650 ^{o}C, attributed to decomposition and degradation of the carbon skeleton.

Besides the former systems showing mass losses in three stages, the thermograms of FeNPs/AN@rGO and FeNPs/PPD@rGO showed two steps mass degradation [Fig. 6]. Here, initial mass loss of 5.6% and 8.2% was observed in the temperature range of 110-280 ^{o}C due to the liberation of un-functionalized oxygen-containing functional groups and the final mass loss of 44.2% and 48.7% was observed in the temperature range of 280-650 ^{o}C that corresponds to degradation of the carbon skeleton.
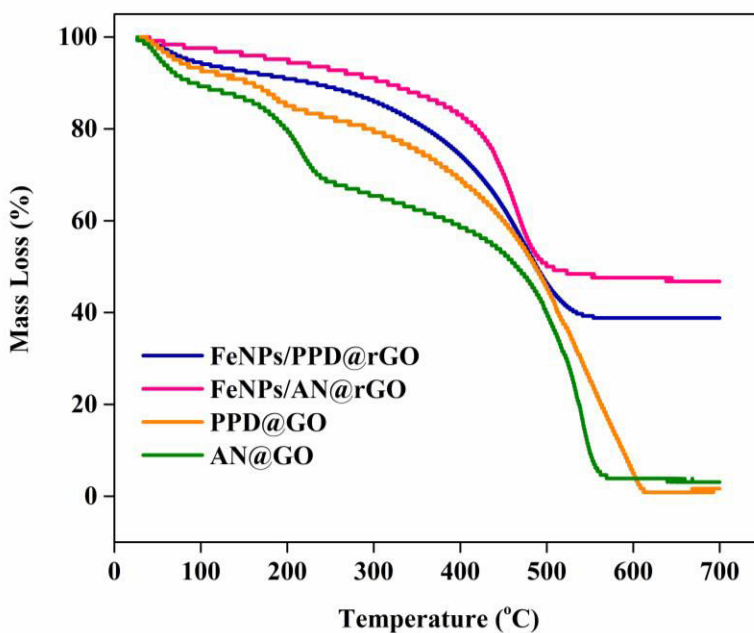

Figure 6 TG analysis of AN@GO, PPD@GO, FeNPs/AN@rGO, FeNPs/PPD@rGO

(g) X-ray Photo electronic Spectroscopy (XPS)

XPS analysis is an imperative technique to investigate the surface chemical composition and bonding environment of the as-prepared nanocatalysts. Fig. 7 shows the XPS survey spectra of PPD@GO and FeNPs/PPD@rGO. The Survey spectra of PPD@GO (Fig. 7), confirms the presence of N elements as an additional peak at ~398 eV besides C and O at ~281 and ~530.Y, respectively. While, the functionalization of GO with PPD, new peak was observed at 398.7 attributing to C-N bond of the amide formation via reaction of PPD with carboxyl groups of GO. Moreover, covalent attachment of FeNPs in the subsequent step was also confirmed in the survey spectra of FeNPs/PPD@rGO as an additional peak at 710 eV and besides the custom peaks of C, O and N at ~281, ~530 and ~400 eV, respectively.

In the C1s spectra of FeNPs/PPD@rGO (Fig. 7), intensity of peaks observed at 288.6, 289.8 and 289.6 eV in GO (depicted in chapter 2, fig. 9) was decreased remarkably, contrary to the peak at 286.6 in GO which was increased. This is due to the re-establishment of new in-plane sp^2 domains, having good concurrence with Raman spectral studies. However, on formation of amide groups by the reaction of PPD with carboxyl groups of GO, the intensity of –COOH groups was decreased markedly.

Consequently, the high-resolution N 1s spectrum of FeNPs/PPD@rGO (Fig. 7) exhibited two peaks at 398.4 and 400.4 eV, attributing to the formation of –CO–NH and CH_2NH_2, respectively. This supports the above verdict of FeNPs/PPD@rGO C 1s spectra. Moreover, the binding energy of iron is exhibited at 713.5 and 725.3 eV (Fig. 7), suggesting the existence of Fe $2p_{3/2}$ and Fe $2p_{5/2}$, respectively which clearly illustrated that FeNPs is successfully attached on the surface of GO nanosheet. These results imply that there are no impurities present within the sample.
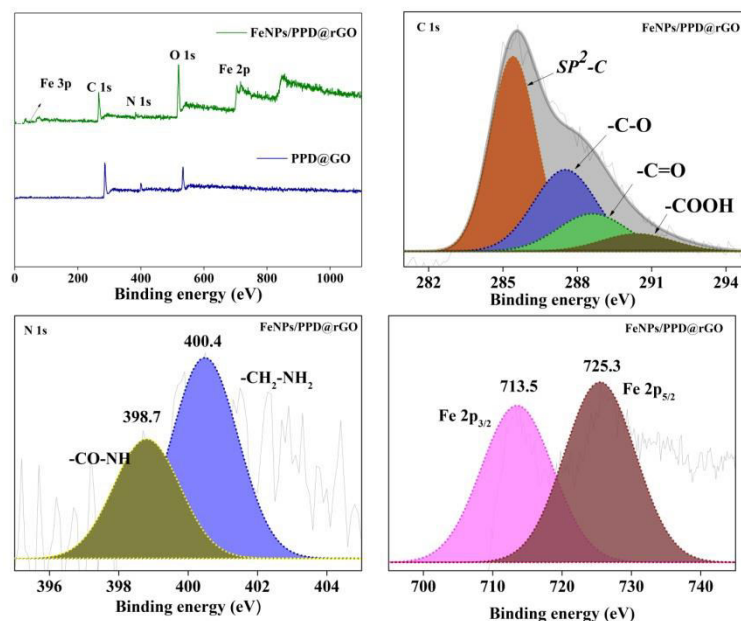
Figure 7 XPS spectra, survey spectra of PPD@GO, FeNPs/PPD@rGO, C 1s spectra of FeNPs/PPD@rGO, N 1s spectra of FeNPs/PPD@rGO, Fe 2p core level spectrum.

[5.4]   Catalytic study

The catalytic performance of as-prepared nanocatalysts was assessed by the Knoevenagel condensation reaction using benzaldehyde as starting material with active methylene compound i.e. malononitrile and toluene as a non-polar solvent to form benzylidene malononitrile as the principle product (Scheme 2).
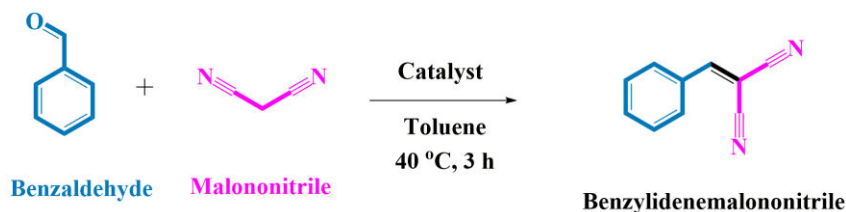
Scheme 2 A schematic representation of Knoevenagel condensation reaction.

In typical reaction conditions, benzaldehyde and malononitrile in 1:1 mole ratio were dissolved in 5 mL toluene and refluxed for 3 h at 40 ^{o}C using 20 mg (0.11 mol% of Fe) catalyst. GO, PPD, AN, PPD@GO, AN@GO, solid acid-base bifunctional nanocatalysts i.e. FeNPs/PPD@rGO and/or FeNPs/AN@rGO was

investigated for Knoevenagel condensation reaction and the results are depicted in Fig. 8. It was clearly observed from the figure that GO showed minute conversion while PPD and AN exhibited comparatively enhanced conversion of benzaldehyde. However, PPD@GO and AN@GO showed not much higher conversion than that of pristine GO, PPD and AN. Through FeNPs/PPD@rGO and FeNPs/AN@rGO catalysts, higher catalytic conversions of benzaldehyde (i.e. 86.2% & 80.5%) were observed with 84.55% & 76.85% yield of benzylidenemalononitrile, respectively. These outcomes support the crucial role of FeNPs as Lewis acid which leads to the formation of aldimine by activating carbonyl group of aldehyde.[69] Amongst the two solid acid-base nanocatalysts (FeNPs/PPD@rGO and FeNPs/AN@rGO), FeNPs/PPD@rGO was found to be a potential contender, offering outstanding conversion and superior yield of product that might be due to presence of highest number of nitrogen sites (-NH-, and –NH$_2$). [70] However, we have performed the elemental analysis for N content in AN@GO, PPD@GO, FeNPs/AN@rGO and FeNPs/PPD@rGO and the obtained results are 3.9, 7.9, 4.0 and 8.1%, respectively. The result confirms higher N content in FeNPs/PPD@rGO (i.e. 8.1%). Hence, FeNPs/PPD@rGO is considered as a representative nanocatalyst for further investigation.
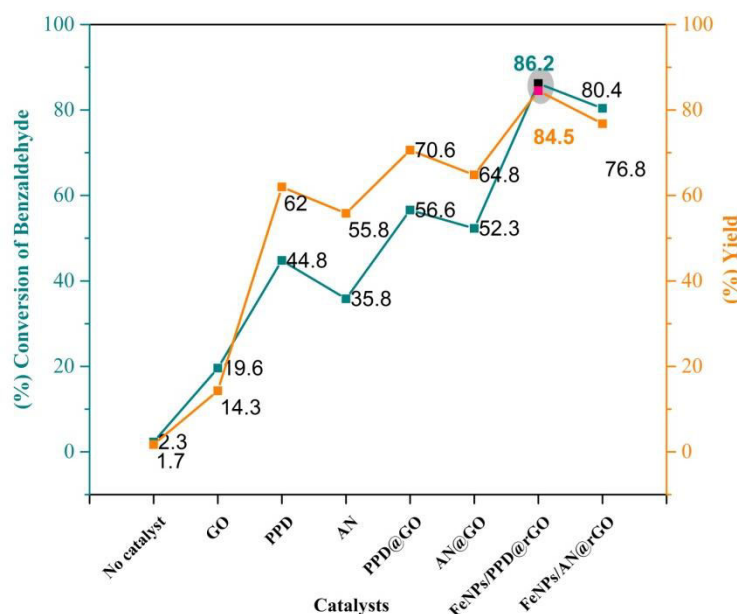
Figure 8 The catalytic activity of various catalysts over Knoevenagel condensation reaction. (adapted from Ref. 82 with permission of Royal Society of Chemistry)
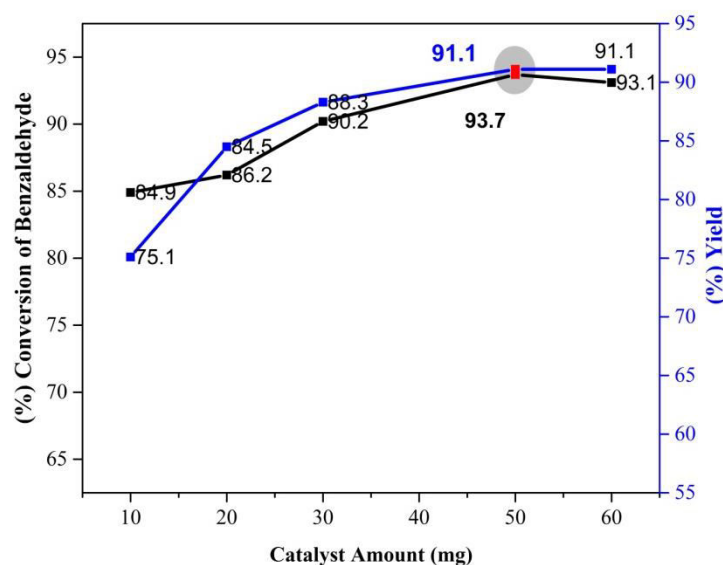
Reaction condition: Benzaldehyde (5 mmol), Malononitrile (5 mmol), **Varying Catalysts** (20 mg, 0.11 mol% of Fe), Toluene (5 ml), Temp. (40 ^{o}C), Time (3 h).

✦ **Factor affecting the Knoevenagel Condensation reaction**

(a)   Effect of catalyst dosage

The catalyst dosage is one of the leading factors in Knoevenagel condensation reaction. We have inspected the impact of catalyst dosages on the aforesaid reaction by keeping other parameters fixed. As shown in Fig. 9, a representative catalyst FeNPs/PPD@rGO with five different dosages viz. 10 (0.05 mol% of Fe), 20 (0.11 mol% of Fe), 30 (0.17 mol% of Fe), 50 (0.28 mol% of Fe), 60 mg (0.34 mol% of Fe) was employed. Among them, the uppermost of 91.2% benzaldehyde conversion with 93.8% yield of the product was monitored with 50 mg (0.28 mol% of Fe) of catalyst dosage.

A further augment in catalyst dosage observed no significant difference in conversion as well as yield. Therefore, the optimum dosage of the catalyst is considered to be 50 mg (0.28 mol% of Fe) for the further investigation.

a: (10, 0.05 mol% of Fe); **b**: (20, 0.11 mol% of Fe), **c**: (30, 0.17 mol% of Fe); **d**: (50, 0.28 mol% of Fe); **e**: (60 mg, 0.34 mol% of Fe).

Figure 9 The effect of catalyst dosage in the Knoevenagel condensation reaction.

(adapted from Ref. 82 with permission of Royal Society of Chemistry)

Reaction condition: Benzaldehyde (5 mmol), Malononitrile (5 mmol), FeNPs/PPD@rGO (**X mg**), Toluene (5 ml), Temp. (40 ^{o}C), Time (3 h).

(b)   Effect of mole ratio

For this archetypal condensation reaction, we have gone through one more crucial aspect i.e. mole ratio. The impact of varying mole ratio of benzaldehyde to malononitrile was investigated by employing four different mole ratios such as 1:1, 1:1.5, 1:2, and 1: 2.5.

As shown in Fig. 10, utmost 97.1% conversion of benzaldehyde with 96.7% yield of product was achieved with mole ratio of 1:1.5. Furthermore, increase in the concentration of active methylene group resulted into reduction of benzaldehyde conversion along with yield of product. Aforesaid reduction was believed to be due to self-condensation process within active methylene compounds. [71] Accordingly, the mole-ratio 1:1.5 is considered as representative for farther optimization of remaining parameters.
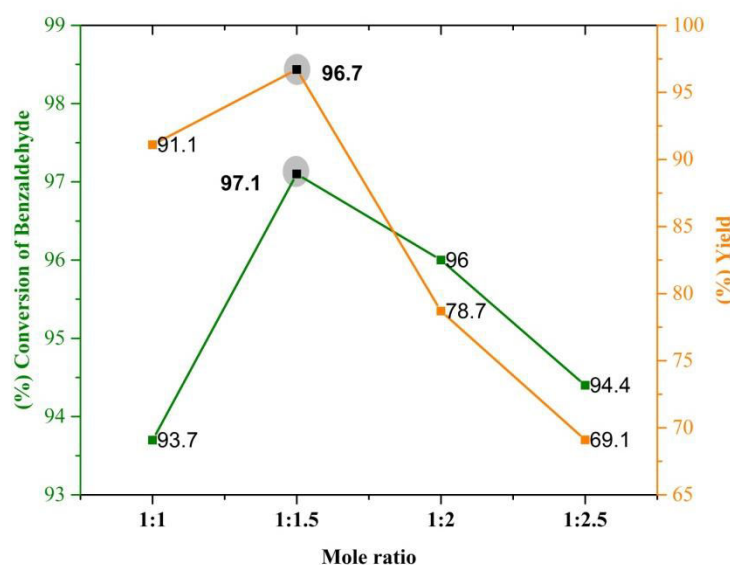
Figure 10 The effect of mole ratio (Benzaldehyde: malononitrile) in the Knoevenagel condensation reaction. (adapted from Ref. 82 with permission of Royal Society of Chemistry)

Reaction condition: Benzaldehyde (5 mmol), Malononitrile (**X mmol**), FeNPs/PPD@rGO (50 mg, 0.28 mol% of Fe), Toluene (5 ml), Temp. (40 ^{o}C), Time (3 h).

(c)   Effect of solvent

The effect of discrete solvents such as methanol, acetonitrile and toluene was studied for this aforementioned condensation reaction by keeping other parameters fixed. As shown in Fig. 11, conversion of benzaldehyde and yield of product was seen to be decreasing in the order of: toluene (97.1%, 96.7%) > methanol (94.8%, 83.8%) > acetonitrile (92.3%, 85.5%). Methanol and acetonitrile have given comparably lower conversion and yield of product as most likely to be due to self-condensation and oligomerization reactions of the primary reaction product. Among them, toluene with excellent dilution factor offers superior conversion and yield and that's why taken as preferred solvent for the further experiments. [72]
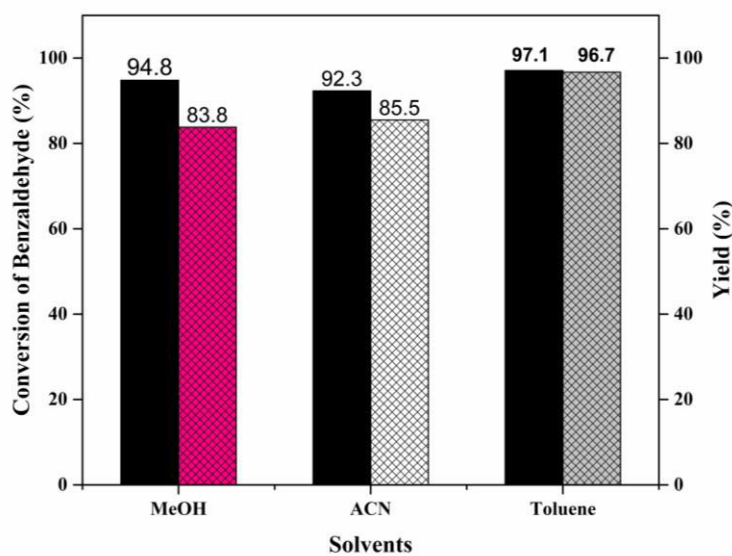
117

Figure 11 The effect of various solvents in the Knoevenagel condensation reaction. (adapted from Ref. 82 with permission of Royal Society of Chemistry)

Reaction condition: Benzaldehyde (5 mmol), Malononitrile (7.5 mmol), FeNPs/PPD@rGO (50 mg, 0.28 mol% of Fe), **various solvents** (5 ml), Temp. (40 ^{o}C), Time (3 h).

(d)   Effect of Temperature

The catalytic conversion and yield of the reaction were influenced by discrete temperature (Fig. 12). As perceiving, the general trend of increasing reaction temperature raises substrate conversion, while during change of temperature from ambient to 40, 50, 75 and up to reflux temperature, the said trend was observed. On contrary to this, reciprocal trend was exhibited in yield formation. Maximum yield of 96.7% achieved at 40 ^{o}C but however, the yield showed drastic reduction of 8.2% while increasing the temperature. This reduction was probably due to the formation of by-products via ensuing self-condensation and oligomerization reactions of the primary reaction product. Looking at the conversion, 97.1% was achieved at 40 ^{o}C and increase in temperature showed increment of only 2.8% which was quite lowered than the reduction in the yield. As a result, the reaction temperature was fixed at 40 ^{o}C for further optimization.
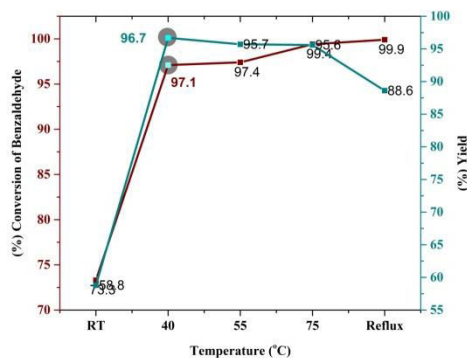
Figure 12 The effect of various temperatures in the Knoevenagel condensation reaction. (adapted from Ref. 82 with permission of Royal Society of Chemistry)

Reaction condition: Benzaldehyde (5 mmol), Malononitrile (7.5 mmol), FeNPs/PPD@rGO (50 mg, 0.28 mol% of Fe), Toluene (5 ml), **Temp.** (**X ^{o}C**), Time (3 h).

(e)   Effect of Time

The influence of reaction time is a significant factor throughout the reaction that enables us to determine the optimal time for achieving desired conversion and yield. As shown in Fig. 13, it was noticed that both conversion and yield increased with preceding reaction time and reached maximum i.e. 100 % in 3.5 h. However, the reaction time was prolonged for 4 h; there was no change in conversion and yield of the product. For the same, we have chosen maximum time 3.5 h for this condensation reaction to check further parameters.
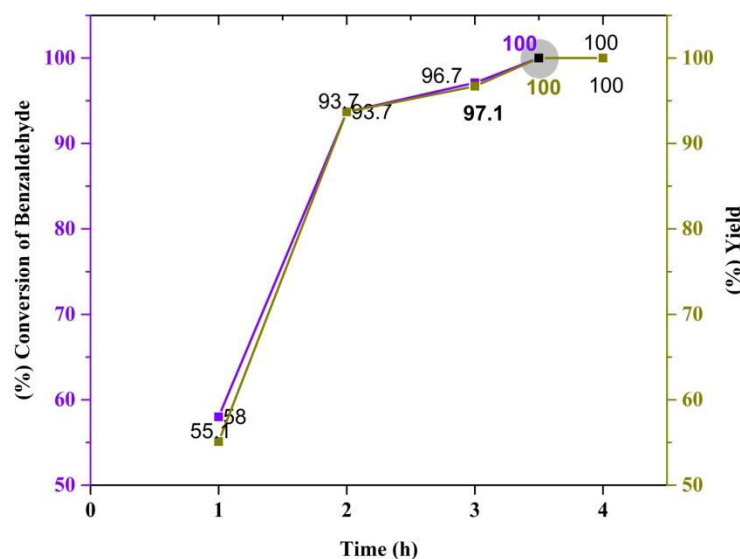
Figure 13 The effect of various times in the Knoevenagel condensation reaction. (adapted from Ref. 82 with permission of Royal Society of Chemistry)
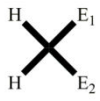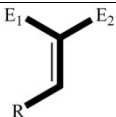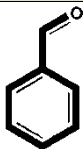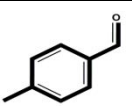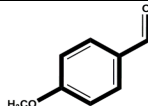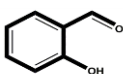
Reaction condition: Benzaldehyde (5 mmol), Malononitrile (7.5 mmol), FeNPs/PPD@rGO (50 mg, 0.28 mol% of Fe), Toluene (5 ml), Temp. (40 ^{o}C), **Time (X h).**
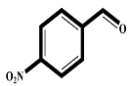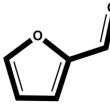
[5.5] Knoevenagel Condensation reaction using diverse aldehydes with active methylene compounds over FeNPs/PPD@rGO as a representative nanocatalyst

After accomplishing optimized conditions for the aforesaid condensation reaction, possibility and limitations of FeNPs/PPD@rGO catalyst were extended and investigated among diverse aldehyde derivatives and active methylene compounds. As shown in Table 1, benzaldehyde reacted fruitfully with active methylene compounds (such as malononitrile, ethyl cyanoactate, and ethyl acetoacetate) to give corresponding benzylidene products. Taking FeNPs/PPD@rGO as a representative catalyst with toluene as a solvent, the reaction was completed within 3.5 h (Table 1, entry 1). Moreover, various aromatic aldehydes including electron-withdrawing (such as 4-methyl benzaldehyde, 4- methoxy benzaldehyde and 2-hydroxy benzaldehyde), electron donating (4-nitro benzaldehyde) and hetero atom (furfuryldehyde) groups reacted with active methylene compounds to furnish Knoevenagel products with excellent

conversion and yield (Table 1, entry 2-6). Looking to the observed results (Table 1), the electron withdrawing groups have shown superior conversion and yield except 2-hydroxy benzaldehyde which has shown slightly lower reactivity owing to their steric hindrance. [68] Furthermore, electron donating group with an active methylene compounds exhibited same trend as of 2-hydroxy benzaldehyde. [68] Steric hindrance largely affects reactant derivative conversion as ortho-substituted derivative has deprived results than that of p- and m- substituted derivatives with no desired product achieved. In addition to this, we investigated furfuryldehyde with active methylene compounds which was transformed to the desired product with excellent conversion and yield of product (Table 1).

Table 1 The Knoevenagel condensation reaction of different aldehydes with active methylene compounds over Fe/PPD@rGO nanocatalyst.

Entry	Substract (A)	Active methylene Compounds		Conversion (%)	Yield (%)	TON	TOF (h^{-1})
		E$_1$	E$_2$				
1		-CN	-CN	100	100	350.8	100.2
		-CN	-COOCH$_2$CH$_3$	79.4	23.7	278.8	79.6
		-COCH$_3$	-COOCH$_2$CH$_3$	78.5	20.6	275.8	78.7
2		-CN	-CN	60.0	92.5	210.5	60.1
		-CN	-COOCH$_2$CH$_3$	33.1	4.1	116.1	33.1
		-COCH$_3$	-COOCH$_2$CH$_3$	27.8	1.9	97.8	27.9
3		-CN	-CN	58.2	99.7	204.5	58.4
		-CN	-COOCH$_2$CH$_3$	56.0	43.1	196.7	56.1
		-COCH$_3$	-COOCH$_2$CH$_3$	50.4	38.6	177.1	50.6
4		-CN	-CN	47.0	14.2	164.9	47.1
		-CN	-COOCH$_2$CH$_3$	20.8	1.1	73.2	20.9
		-COCH$_3$	-COOCH$_2$CH$_3$	10.5	0.8	37.1	10.6

|							
5		-CN	-CN	53.8	4.4	189.0	54.0
		-CN	-COOCH$_2$CH$_3$	27	1.8	94.8	27.0
		-COCH$_3$	-COOCH$_2$CH$_3$	21.1	1.5	47.0	21.1
6		-CN	-CN	98.4	85.8	345.2	98.6
		-CN	-COOCH$_2$CH$_3$	38.7	2.8	135.8	38.8
		-COCH$_3$	-COOCH$_2$CH$_3$	37.9	1.6	132.9	37.9

Reaction condition: Benzaldehyde (5 mmol), Malononitrile (7.5 mmol), FeNPs/PPD@rGO (50 mg, 0.28 mol% of Fe), Toluene (5 ml), Temp. (40 ^{o}C), Time (3.5 h).

[c]TON (turnover number) = Moles of desired product formed/moles of catalyst.

[d]TOF (turnover frequency) = Turnover number (TON)/hours

[5.6] The plausible reaction mechanism for Knoevenagel condensation reaction using FeNPs/PPD@rGO as a representative catalyst

The plausible reaction mechanism for the Knoevenagel condensation reaction using FeNPs/PPD@rGO as a representative catalyst has shown in Scheme 3. From spectroscopic results, acid-base sites present in FeNPs/PPD@rGO nanocatalyst proved to be acting crucially in the aforesaid reaction. The probable role of acidic and basic sites in the reaction mechanism can be given as: Fe nanoparticles act as acidic sites; while NH$_2$ groups of PPD act as basic sites. Both these sites simultaneously activate the carbonyl group of benzaldehyde substrate and forms aldimine intermediate species which is generally stronger than amine and more reactive than primary aldehyde. [20,73] As a result, this intermediate skillfully activates the methylene groups, followed by the addition-elimination reactions leading to the formation of desired product. Therefore, the role of acid and base sites present on the catalyst surface is very crucial in achieving the superior performance for this condensation reaction. Hence, we have prepared such catalyst consisting of both acidic and basic sites. [69]
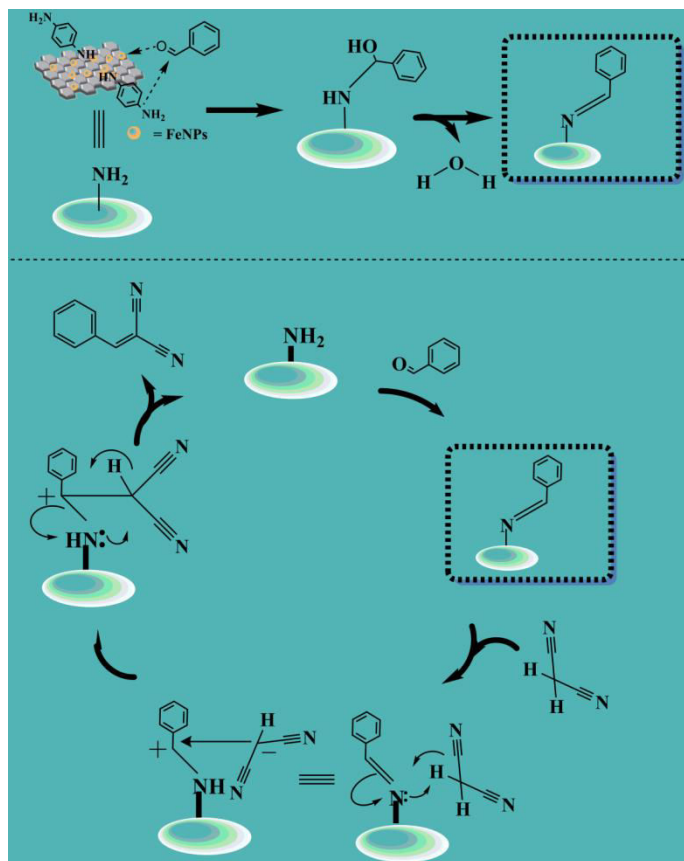
Scheme 3 The plausible reaction mechanism for the Knoevenagel condensation reaction using FeNPs/PPD@rGO nanocatalyst. (adapted from Ref. 82 with permission of Royal Society of Chemistry)

[5.7]   Recyclability test

The recyclability of the as-prepared catalyst in the aforementioned condensation reaction was also examined under standard optimized conditions (Fig. 13). The catalyst was recovered by centrifugation after each cycle and it has been recycled up to six times, showing better catalytic activity up to 5 cycles without any significant loss of activity, though in the 6th run the conversion and yield was drop downed to 97.9% and 90%, respectively. This loss of activity was believed to be due to metal leaching during the recovery process and reaction. Hence, to corroborate, we have performed ICP analysis of the heterogeneous catalyst (FeNPs/PPD@rGO) before and after recycle experiments. The results confirmed the leaching of FeNPs with loss of 0.021%.
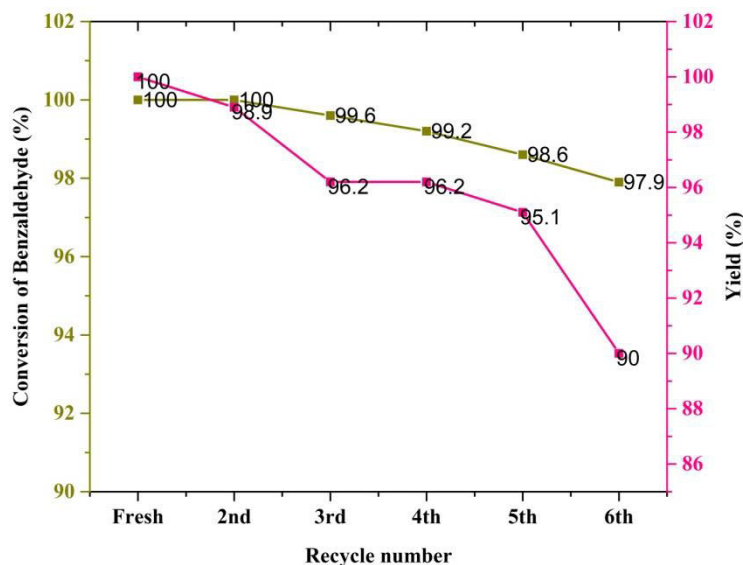
Fig. 13 Recyclability of FeNPs/PPD@rGO in the Knoevenagel condensation reaction (adapted from Ref. 82 with permission of Royal Society of Chemistry)

Reaction condition: Benzaldehyde (5 mmol), Malononitrile (7.5 mmol), FeNPs/PPD@rGO (50 mg, 0.28 mol% of Fe), Toluene (5 ml), Temp. (40 °C), Time (3.5 h).

[5.8]   Comparative Study

No.	Catalysts	Solvent	Temp. (°C)	Time (h)	Conversion (%)	[c]TON	[d]TOF (h[-1])	Reference
1	MOF-NH$_2$	DMF	80	4.5	51	--	--	[74]
2	Ce(PO$_2$NH)$_3$.5H$_2$O	Ethanol	100	2	95	--	--	[75]
3	Pb(cpna)$_2$.2DMF.6H$_2$O	CH$_3$CN	R.T.	24	100	--	--	[76]
4	Chitosan	Ethanol	40	6	99	--	--	[77]
5	[a]Cata.-A	--	60	6	95	193	--	[78]
	[b]Cata.-B	--	60	6	93	186	--	
6	Amino-functionalized mesoporous silica	Ethanol	R.T.	6	90	--	5.2	[7]

7	$Ce_{0.4}Bi_{0.6}O_{1.7}$	Ethanol	35	6	100	--	9	[79]
8	DCN	--	40	2	17.4	37	--	[80]
9	PIM-TB-Trip-1	--	18	2	100	37	2.5	[81]
10	FeNPs/PPD@rGO	Toluene	40	3.5	100	350.8	100.2	This Work

Table 2 Comparison study

[a]Catal.-A = {[Co_2(1,4-NDC)$_2$([3,3'-azobis(pyridine)])(H$_2$O)$_2$ (μ^2-H$_2$O)]·(DMF)$_2$(H$_2$O)}$_n$,

[b]Catal.-B = {[Co(fma)([3,3'-azobis(pyridine)])(H$_2$O)$_2$]·S}$_n$,

[c]TON (turnover number) = Moles of desired product formed/moles of catalyst.

[d]TOF (turnover frequency) = Turnover number (TON)/hours.

The catalytic Knoevenagel condensation reaction using varying homogeneous and/or heterogeneous systems has been studied previously by some other groups are discussed and tabulated in Table 2. A. Taher and co-workers [74] reported the Knoevenagel condensation reaction using MOF-NH$_2$ as an efficient catalyst and DMF as a solvent at 80 $^{\circ}$C, achieving 51% benzaldehyde conversion at 4.5 h (Table 2, Entry 1). J L Yi and co-workers [75] developed Ce(PO$_2$NH)$_3$.5H$_2$O catalyst for Knoevenagel condensation reaction, using ethanol as solvent system they observed 95% conversion of benzaldehyde at 100 $^{\circ}$C (Table 2, Entry 2). X. M. Lin et al. [76] using Pb(cpna)$_2$.2DMF.6H$_2$O as a catalyst with CH$_3$CN as a solvent inspected maximum 100% conversion of benzaldehyde after 24 h at room temperature (Table 2, Entry 3). B. Shakhtivel and co-workers [77] reported the said condensation reaction catalyzed by Chitosan using ethanol as a solvent at 40 $^{\circ}$C for 6 h, achieving 99% conversion of benzaldehyde (Table 2, Entry 4). S. Chand et al. [78] developed an efficient two catalysts viz. catal.-A: [{[Co$_2$(1,4-NDC)$_2$([3,3'-azobis(pyridine)])(H$_2$O)$_2$(μ_2-H$_2$O)]·(DMF)$_2$(H$_2$O)}$_n$] and catal.-B: [{[Co(fma)([3,3'-azobis(pyridine)])(H$_2$O)$_2$]·S}$_n$] for Knoevenagel condensation reaction under 60 $^{\circ}$C Temperature for 6 h, they achieved 95% and 93% yield with TON value of 193 and 186, respectively (Table 2, Entry 5). J. Mondal co-workers [7] reported that the Knoevenagel condensation reaction

catalyzed by amino functionalized mesoporous silica in presence of ethanol at R.T. for 6 h, they observed 90% yield with TOF (h^{-1}) value of 5.2 (Table 2, Entry 6). The mixture of Ce-based and Bi-based BiCe oxide developed by G. Varga and co-workers [79] and used in the Knoevenagel condensation reaction under ethanol as solvent at 35 ^{o}C for 6 h. This system achieved the highest 100% conversion of benzaldehyde with TOF (h^{-1}) value of 9.0 (Table 2, Entry 7). DCN was taken as catalyst for the Knoevenagel condensation reaction by L. Zhang and co-worker, [80] achieving 17.4% conversion with TON value of 37 (Table 2, Entry 8). M. Carta et al. [81] used microporous polymer catalyst PIM-TB-Trip-1 for the Knoevenagel condensation reaction, they achieved 100% yield at 18 ^{o}C for 2 h. and they also calculated TON and TOF (h^{-1}) value of 37 and 2.5 (Table 2, Entry 9). In this article, we have developed a catalytic system FeNPs/PPD@rGO for the Knoevenagel condensation reaction employing toluene as a solvent at nearly ambient temperature (40 ^{o}C) for inferior time i.e. 3.5 h, showing superior 100% benzaldehyde conversion with 100% yield of the product and also calculated TON and TOF (h^{-1}) are 350.8 and 100.2 (Table 2, Entry 10).

[5.9] Conclusions

In concluding remarks, we have adequately developed an effortless and skilful blueprint for the synthesis of FeNPs anchored on amino modified rGO (FeNPs/Am@rGO) as bifunctional nanocatalysts for the first time, presenting amino based organic chunk on the basal and/or edges sites of rGO offering a base peculiarity and FeNPs implanted onto the surface of rGO furnishing Lewis acidic behaviour. FeNPs/Am@rGO exhibited exceptional catalytic activity and selectivity in one-pot Knoevenagel condensation reaction. Amongst them, FeNPs/PPD@rGO manifested gloriously enhanced catalytic efficiency leading to 100% benzaldehyde conversion with exceptional 100% yield of product. This extraordinarily high catalytic activity could be ascribed to the combined effects of acid-base supportive catalytic aptitude and the unique two-dimensional open structure offered by graphene support. The plausible catalytic mechanism for the aforesaid condensation reaction proposed in two catalogues: Activation of substrate carbonyl group using bifunctional catalyst forming highly reactive

aldimine intermediate species, pursued by deprotonation of methylene compound through intermediate species generating the desired final product along with regeneration of catalyst. This metal nanoparticles implanted amino modified rGO-based acid-base bifunctional catalyst is anticipated to concrete the plan of new circumstances in the growth of highly active and recyclable heterogeneous multifunctional catalysts for new-fangled chemical metamorphosis.

[5.10] References

[1]   F. Freeman, *Chem. Rev.*, **80**, 329 (1980).

[2]   G. A. Kraus, M. E. Krolski, *J. Org. Chem.*, **51**, 3347 (1986).

[3]   L. F. Tietze, N. Rackelmann, *Pure Appl. Chem.* , (2004), 76, 1967.

[4]   F. Liang, Y.-J. Pu, T. Kurata, J. Kido, H. Nishide, *Polymer*, **46**, 3767 (2005).

[5]   D. Kryszak, K. Stawicka, M. Trejda, V. Calvino-Casilda, R. Martin-Aranda, M. Ziolek, *Catal. Sci. Technol.*, **7**, 5236 (2017).

[6]   M. Fujita, Y. J. Kwon, S. Washizu, K. Ogura, *J. Am. Chem. Soc.*, **116**, 1151 (1994).

[7]   J. Mondal, A. Modak, A. Bhaumik, *J. Mol. Catal. A Chem.*, **335**, 236 (2011).

[8]   R. Xing, H. Wu, X. Li, Z. Zhao, Y. Liu, L. Chen, P. Wu, *J. Mater. Chem.*, **19**, 4004 (2009).

[9]   K. M. Parida, S. Mallick, P. C. Sahoo, S. K. Rana, *Appl. Catal. A Gen.*, **381**, 226 (2010).

[10]   Z. Gao, J. Zhou, F. Cui, Y. Zhu, Z. Hua, J. Shi, *Dalt. Trans.*, **39**, 11132 (2010).

[11]   B. Karmakar, B. Chowdhury, J. Banerji, *Catal. Commun.,* **11**, 601 (2010).

[12]   F. Shang, J. Sun, S. Wu, Y. Yang, Q. Kan, J. Guan, *Microporous Mesoporous Mater.*, **134**, 44 (2010).

[13]   W. Jiang, J. Yang, Y.-Y. Liu, S.-Y. Song, J.-F. Ma, *Inorg. Chem.*, **56**, 3036 (2017).

[14]   G. Postole, B. Chowdhury, B. Karmakar, K. Pinki, J. Banerji, A. Auroux,

J. Catal., **269**, 110 (2010).

[15]   L. Martins, K. M. Vieira, L. M. Rios, D. Cardoso, *Catal. Today*, **133**–**135**, 706 (2008).

[16]   F. Guo, *Inorg. Chem. Commun.***101**, 87 (2019).

[17]   K. R. Reddy, K. Rajgopal, C. U. Maheswari, M. Lakshmi Kantam, *New J. Chem.*, **30**, 1549 (2006).

[18]   X.-W. Feng, C. Li, N. Wang, K. Li, W.-W. Zhang, Z. Wang, X.-Q. Yu, *Green Chem.*, **11**, 1933 (2009).

[19]   M. Trilla, R. Pleixats, M. W. C. Man, C. Bied, *Green Chem.*, **11**, 1815 (2009).

[20]   J. Gascon, U. Aktay, M. D. Hernandez-Alonso, G. P. M. van Klink, F. Kapteijn, *J. Catal.*, **261**, 75 (2009).

[21]   U. P. N. Tran, K. K. A. Le, N. T. S. Phan, *ACS Catal.*, **1**, 120 (2011).

[22]   Y.-B. Huang, J. Liang, X.-S. Wang, R. Cao, *Chem. Soc. Rev.*, **46**, 126 (2017).

[23]   H. Li, Q. Pan, Y. Ma, X. Guan, M. Xue, Q. Fang, Y. Yan, V. Valtchev, S. Qiu, *J. Am. Chem. Soc.*, **138**, 14783 (2016).

[24]   H. Wang, C. Wang, Y. Yang, M. Zhao, Y. Wang, *Catal. Sci. Technol.*, **7**, 405 (2017).

[25]   H. Li, J. He, A. Riisager, S. Saravanamurugan, B. Song, S. Yang, *ACS Catal.*, **6**, 7722 (2016).

[26]   J. Du, M. Tao, W. Zhang, *ACS Sustain. Chem. Eng.*, **4**, 4296 (2016).

[27]   M. A. Ali, S. M. A. H. Siddiki, K. Kon, K. Shimizu, *ChemCatChem*, **7**, 2705 (2015).

[28]   M. Golestanzadeh, H. Naeimi, Z. Zahraie, *Mater. Sci. Eng. C. Mater. Biol. Appl.*, **71**, 709 (2017).

[29]   M. Golestanzadeh, H. Naeimi, *ChemistrySelect*, **4**, 1909 (2019).

[30]   Q. Zhao, H. Wang, H. Zheng, Z. Sun, W. Shi, S. Wang, X. Wang, Z. Jiang, *Catal. Sci. Technol.*, **3**, 2204 (2013).

[31]   J. Zhao, B. Lin, Y. Zhu, Y. Zhou, H. Liu, *Catal. Sci. Technol.*, **8**, 5900 (2018).

[32] L. Xiong, H. Zhang, Z. He, T. Wang, Y. Xu, M. Zhou, K. Huang, *New J. Chem.*, **42**, 1368 (2018).

[33] O. Mohammadi, M. Golestanzadeh, M. Abdouss, *ChemistrySelect*, **3**, 12131 (2018).

[34] O. Mohammadi, M. Golestanzadeh, M. Abdouss, *New J. Chem.*, **41**, 11471 (2017).

[35] M. Golestanzadeh, H. Naeimi, Z. Zahraie, *ChemistrySelect*, **1**, 6490 (2016).

[36] F. Zhang, H. Jiang, X. Li, X. Wu, H. Li, *ACS Catal.*, **4**, 394 (2014).

[37] A. Bahuguna, S. Kumar, V. Sharma, K. L. Reddy, K. Bhattacharyya, P. C. Ravikumar, V. Krishnan, *ACS Sustain. Chem. Eng.*, **5**, 8551 (2017).

[38] N. M. Julkapli, S. Bagheri, *Int. J. Hydrogen Energy*, **40**, 948 (2015).

[39] X. Li, W.-X. Chen, J. Zhao, W. Xing, Z.-D. Xu, *Carbon N. Y.*, **43**, 2168 (2005).

[40] G. Eda, G. Fanchini, M. Chhowalla, *Nat. Nanotechnol.*, **3**, 270 (2008).

[41] L. Q. Lu, L. J. Lu, Y. Wang, *J. Mater. Chem. A*, **1**, 9173 (2013).

[42] J. Huang, S. Ding, W. Xiao, Y. Peng, S. Deng, N. Zhang, *Catal. Letters*, **145**, 1000 (2015).

[43] R. Vithalani, D. Patel, C. K. Modi, N. N. Som, P. K. Jha, S. R. Kane, *Diam. Relat. Mater.*, **90**, 154 (2018).

[44] A. Bahuguna, A. Kumar, T. Chhabra, A. Kumar, V. Krishnan, *ACS Appl. Nano Mater.*, **1**, 6711 (2018).

[45] Y. Zhu, S. Murali, W. Cai, X. Li, J. W. Suk, J. R. Potts, R. S. Ruoff, *Adv. Mater.*, **22**, 3906 (2010).

[46] B. Paulchamy, G. Arthi, B. D. Lignesh, *J Nanomed Nanotechnol*, **6**, 253 (2015).

[47] A. C. Ferrari, *Solid State Commun.*, **143**, 47 (2007).

[48] A. C. Ferrari, D. M. Basko, *Nat. Nanotechnol.*, **8**, 235 (2013).

[49] J. B. Wu, X. Zhang, M. Ijas, W. P. Han, X. F. Qiao, X. L. Li, D. S. Jiang, A. C. Ferrari, P. H. Tan, *Nat. Commun.*, **5**, 5309 (1-8) (2014).

[50] S. Mondal, S. Sudhu, S. Bhattacharya, S. K. Saha, *J. Phys. Chem. C*, **119**,

27749 (2015).

[51]   X. Sheng, W. Cai, L. Zhong, D. Xie, X. Zhang, *Ind. Eng. Chem. Res.*, **55**, 8576 (2016).

[52]   P. Bandyopadhyay, T. Kuila, J. Balamurugan, T. T. Nguyen, N. H. Kim, J. H. Lee, *Chem. Eng. J.*, **308**, 1174 (2017).

[53]   P. Bandyopadhyay, W. B. Park, R. K. Layek, M. E. Uddin, N. H. Kim, H.-G. Kim, J. H. Lee, *J. Memb. Sci.*, **500**, 106 (2016).

[54]   F. Tuinstra, J. L. Koenig, *J. Chem. Phys.*, **53**, 1126 (1970).

[55]   M. Mishra, F. Meinerzhagen, M. Schleberger, D. Kanjilal, T. Mohanty, *J. Phys. Chem. C*, **119**, 21270 (2015).

[56]   H.-J. Shin, K. K. Kim, A. Benayad, S.-M. Yoon, H. K. Park, I.-S. Jung, M. H. Jin, H.-K. Jeong, J. M. Kim, J.-Y. Choi, Y. H. Lee, *Adv. Funct. Mater.*, **19**, 1987 (2009).

[57]   S. Moussa, A. R. Siamaki, B. F. Gupton, M. S. El-Shall, *ACS Catal.*, **2**, 145 (2012).

[58]   Z.-J. Fan, W. Kai, J. Yan, T. Wei, L.-J. Zhi, J. Feng, Y. Ren, L.-P. Song, F. Wei, *ACS Nano*, **5**, 191 (2011).

[59]   F. Yin, Z. Liu, Y. Zhao, Y. Feng, Y. Zhang, *Nanomater.***7**, 253(1-9) (2017).

[60]   X. Wu, Y. Xing, D. Pierce, J. X. Zhao, *ACS Appl. Mater. Interfaces*, **9**, 37962 (2017).

[61]   J. Kim, L. J. Cote, J. Huang, *Acc. Chem. Res.*, **45**, 1356 (2012).

[62]   I. V Lightcap, P. V Kamat, *Acc. Chem. Res.*, **46**, 2235 (2013).

[63]   C. Xu, J. Du, L. Ma, G. Li, M. Tao, W. Zhang, *Tetrahedron*, **69**, 4749 (2013).

[64]   M. Golestanzadeh, H. Naeimi, *RSC Adv.*, **9**, 27560 (2019).

[65]   J. Shen, B. Yan, M. Shi, H. Ma, N. Li, M. Ye, *J. Mater. Chem.*, **21**, 3415 (2011).

[66]   L. Li, Y. Dou, L. Wang, M. Luo, J. Liang, *RSC Adv.*, **4**, 25658 (2014).

[67]   M. M. Sk, C. Y. Yue, *RSC Adv.*, **4**, 19908 (2014).

[68]   D. Wang, Z. Li, *Catal. Sci. Technol.*, **5**, 1623 (2015).

[69] Y. Yang, H.-F. Yao, F.-G. Xi, E.-Q. Gao, *J. Mol. Catal. A Chem.*, **390**, 198 (2014).

[70] J. B. M. de Resende Filho, G. P. Pires, J. M. G. de Oliveira Ferreira, E. E. S. Teotonio, J. A. Vale, *Catal. Letters*, **147**, 167 (2017).

[71] R. Mondal, S. Riyajuddin, A. Ghosh, S. Ghosh, K. Ghosh, M. Islam, *J. Organomet. Chem.*, **880**, 322 (2018).

[72] H. Reinsch, M. A. van der Veen, B. Gil, B. Marszalek, T. Verbiest, D. de Vos, N. Stock, *Chem. Mater.*, **25**, 17 (2013).

[73] Q. Yang, H.-Y. Zhang, L. Wang, Y. Zhang, J. Zhao, *ACS Omega*, **3**, 4199 (2018).

[74] A. Taher, D.-J. Lee, B.-K. Lee and I.-M. Lee, *Synlett*, **27**, 1433 (2016).

[75] J. Yi, Z. Fu, S. Liao, D. Song, J. Dai, *J. Mater. Chem.*, **21**, 6144 (2011).

[76] X.-M. Lin, T.-T. Li, L.-F. Chen, L. Zhang, C.-Y. Su, *Dalt. Trans.*, **41**, 10422 (2012).

[77] B. Sakthivel, A. Dhakshinamoorthy, *J. Colloid Interface Sci.*, **485**, 75 (2017).

[78] S. Chand, S. C. Pal, M. Mondal, S. Hota, A. Pal, R. Sahoo, M. C. Das, *Cryst. Growth Des.*, **19**, 5343 (2019).

[79] G. Varga, Á. Kukovecz, Z. Kónya, P. Sipos, I. Pálinkó, *J. Catal.*, **381**, 308 (2020).

[80] L. Zhang, H. Wang, W. Shen, Z. Qin, J. Wang, W. Fan, *J. Catal.*, **344**, 293 (2016).

[81] M. Carta, M. Croad, K. Bugler, K. J. Msayib, N. B. McKeown, *Polym. Chem.*, **5**, 5262 (2014).

[82] D. Patel, R. Vithalani, C. K. Modi, *New J. Chem.,* **44**, 2868 (2020).